

Nanostructural changes in bone quality in a mouse model of chronic kidney disease and treatment with calcitonin

E. Montagnino^a, W. Bush^b, J. Bustamante^c, W. Bandara^c, P. Jalaie^c, M.R. Allen^{d,e},
J.M. Wallace^c, T. Siegmund^b, R.K. Surowiec^c^{*,*}, J.A. Howarter^{a,f}^{*,**}

^a School of Materials Engineering, Purdue University, West Lafayette, USA

^b School of Mechanical Engineering, Purdue University, West Lafayette, USA

^c Weldon School of Biomedical Engineering, Purdue University, West Lafayette, USA

^d Indiana University School of Medicine, Indianapolis, USA

^e Roudebush VA Medical Center, Indianapolis, USA

^f School of Sustainability Engineering & Environmental Engineering, Purdue University, West Lafayette, USA

ARTICLE INFO

Dataset link: [Supporting data for "Nanostructural Changes in Bone Quality in a Mouse Model of Chronic Kidney Disease and Treatment with Calcitonin" \(Original data\)](#)

Keywords:

Bone
Mouse model
Chronic kidney disease
Calcitonin
Bone mass
Bone structure
Bone nanostructure
Micro CT
SAXS
WAXS
X-ray scattering
Thermogravimetric analysis

ABSTRACT

Mineral imbalances in the body from chronic kidney disease can impact bone turnover and cause cortical bone loss. Synthetic salmon calcitonin is an FDA-approved treatment for bone fragility observed in diseases such as osteoporosis, and clinical trials have demonstrated a reduction in fractures compared to untreated individuals. This study documents the effects of calcitonin on cortical bone using an in vivo mouse model of chronic kidney disease. Serum BUN and PTH are reported. Calcitonin was found to impact at a dose of 50 IU/kg/day five times a week for five weeks. MicroCT was used to evaluate bone quantity measures, such as cortical porosity, thickness, bone area, and long bone structural geometric parameters. It was found that porosity, thickness, and bone geometry are affected by disease, but not by treatment at the specified regime. Small and wide-angle x-ray scattering (SAXS and WAXS) was used to obtain the nanostructure of the mineral-collagen-water composite, including mineral dimensions, *D*-periodicity and collagen spacing. Data from thermogravimetric analysis (TGA) were used to quantify wt.% of the mineral, collagen, and bound water of each sample. Chronic kidney disease was found to decrease collagen spacing to increase mineral weight fractions, and to reduce loosely bound water. There were no changes from chronic kidney disease on the *D*-Periodicity. Treatment increased the weight percent of collagen, with no effect on other bone quality parameters.

1. Introduction

Chronic kidney disease (CKD) deregulates calcium and phosphorus levels in the body, which directly affects bone turnover, altering the microstructure and material properties of bone (Nickolas et al., 2013, 2008). The murine model for CKD has been well studied and used to assess how disease progression affects cortical and trabecular bone, with more cases of altered cortical bone reported (Zalozyc et al., 2023). Elevated cortical porosity (Lau et al., 2013; McNerny et al., 2019; Metzger et al., 2022; Newman et al., 2023; Tippen et al., 2022) and decreased cortical thickness (Lee et al., 2010; Heveran et al., 2016a, 2019; Moe et al., 2014; Newman et al., 2014) were reproduced effects on bone impacted by CKD. These changes in microstructure are associated with increased bone fragility (Moe et al., 2014; Newman

et al., 2014; Heveran et al., 2016a, 2019; Surowiec et al., 2023). Previous studies have used cortical bone micro structure improvements as an indication of a treatments effect on CKD impaired bone (Moe et al., 2014; Swallow et al., 2022; Sharma et al., 2024; Chiu et al., 2022; Surowiec et al., 2024).

The material properties of cortical bone such as the quantity of the organic and inorganic phases (Currey, 1969; Battaglia et al., 2003; Lopez Franco et al., 2011; Rodriguez-Florez et al., 2015), structure and quality of the phases (Weiner and Wagner, 1998; Wagermaier et al., 2015) and hydration levels (Surowiec et al., 2022), all work towards maintain mechanical stability. Previous studies have worked to identify the changes in bone quality from CKD, with results such as changes in collagen crosslinking (Iwasaki et al., 2011; Allen et al., 2015; Iwasaki

* Corresponding author.

** Corresponding author at: School of Materials Engineering, Purdue University, West Lafayette, USA.
E-mail addresses: rsurowiec@purdue.edu (R.K. Surowiec), howarter@purdue.edu (J.A. Howarter).

et al., 2015), hydration (Newman et al., 2014; Allen et al., 2015; Surowiec et al., 2023), and quality of the mineral matrix (Iwasaki et al., 2015; Heveran et al., 2019).

Calcitonin (CAL) is a mild inhibitor of bone resorption and was an early-generation approach for treatment in postmenopausal osteoporosis treatment to prevent reduction of bone mineral density (Chesnut et al., 2000; Henriksen et al., 2016). A previous ex vivo study using this CKD model had analyzed the treatment outcomes of CAL on CKD-impacted cortical bone (Surowiec et al., 2023). Ex vivo exposure of CAL was reported to have increased the cortical matrix-bound water compared to vehicle-soaked bones, and this response was stronger in diseased bones than in native bones.

Using a CKD mouse model, the present study seeks to advance the understanding of the effects of CKD on bone quality. This study gives insights into the impacts of CAL on CKD-affected cortical bone quantity and quality (Iwasaki et al., 2011; Heveran et al., 2019; Metzger et al., 2020, 2022; Surowiec et al., 2023). We hypothesize that CAL improves key bone structural characteristics at the micro- and nanoscales. Specifically, we ask if and how CAL treatment in healthy and CKD-affected mice:

- affects bone structure parameters as measured by μ CT measurements on femur bones;
- alters bone microstructure (cortical porosity and bone cross-section properties) as computed from μ CT data;
- modulates the nanostructure of the mineral, collagen-water assembly as measured by small-angle x-ray scattering, and wide-angle X-ray scattering ;
- changes bone tissue composition as deduced from thermogravimetric analysis;

2. Methods

2.1. Animals and study design

Protocols were approved by the Indiana University Indianapolis School of Science Institutional Animal Use and Care Committee. 15-week-old male C57BL/6J mice (B6; JAX #000664; $n = 40$) were obtained from Jackson Laboratories (Bar Harbor, ME, USA). Animals were housed in groups of 3 to 5 per cage in an institutionally approved animal facility with 12-hour light/dark cycles, an average temperature of 70 °F, and access to food and water ad libitum. At 16 weeks of age, CKD was induced in a group of mice ($n = 20$) with a casein-based diet (0.9% phosphorus, 0.6% calcium) with 0.2% adenine. The remaining control littermates ($n = 20$) received a purified casein-based diet (0.9% phosphorus, 0.6% calcium) (Envigo Teklad Diets, Madison, WI, USA). After six weeks on the adenine-laced chow, the disease-affected cohort was switched to the control casein-based diet for four weeks (Metzger et al., 2020). Mice were monitored daily during the CKD induction phase and weighed weekly throughout the study. Starting at 26 weeks of age, a subset of the healthy- and disease-affected mice received subcutaneous injections of synthetic salmon calcitonin (Sigma-Aldrich, 05 – 23 – 2401) at a dose of 50/IU/kg/day five times a week for five weeks. In summary, four groups of animals were present: (1) a group of healthy animals receiving no treatment (CON: $n = 10$), (2) a group of healthy animals receiving CAL treatment (CON CAL: $n = 10$), (3) a group of CKD-affected animals receiving no treatment (CKD: $n = 10$), and (4) a group of CKD affected animals receiving CAL treatment (CKD CAL: $n = 9$). At 31 weeks of age, mice were anesthetized using vaporized inhaled isoflurane and euthanized via cardiac exsanguination followed by cervical dislocation. Blood was collected, serum was isolated, and stored at -20 °C for serum biochemistries. Long bones were removed, cleaned of soft tissue, and frozen (-20 °C) wrapped in PBS-soaked gauze until further testing.

2.2. Biochemistry characterization

Cardiac serum collected at euthanasia was assessed for blood urea nitrogen (BUN) and serum 1 to 84 parathyroid hormone (PTH). BUN was measured via colorimetric assay to assess the presence of kidney disease (BioAssay Systems, Hayward, CA, USA), and PTH was measured via ELISA (Immnotopics Quidel, San Diego, CA, USA). All samples were run as duplicates following the manufacturer's dilutions and protocols.

2.3. X-ray micro computed tomography

The fresh-frozen right femora were scanned while hydrated using a nominal isotropic voxel size of 7.9 μ m through an aluminum filter of 0.5 mm ($V = 59$ kV, $I = 167$ μ A) with an angle step rotation of 0.7° and two frames averaged (SkyScan 1272, Bruker, Billerica, MA, USA). The scans were reconstructed (NRecon; Bruker) and rotated to a standard orientation (DataViewer; Bruker). Intracortical analysis was performed using a 0.1 mm region of interest at 50% of femur total length (proximal to distal). The cortical bone image was automatically segmented by applying a global threshold with a lower gray threshold (70) and an upper gray threshold (255), followed by a shrink wrap. The cortical bone region of interest was then evaluated (CTan; Bruker) for bone structure parameters: total area (T.Ar), cortical area (Ct.Ar), and cortical thickness (Ct.Th). The microstructure of bone was characterized as cortical porosity (Ct.Po) and as bone area fraction (BA/TA=Ct.Ar/T.Ar). The cortical diameter CT.Dia is calculated by a thin-wall approximation such that

$$\text{Ct.Dia} = \frac{\text{Ct.Ar}}{\pi \text{Ct.Th}} \quad (1)$$

The cross-section modulus of inertia (CSMI) is then given as

$$\text{CMSI} = \pi \left(\frac{\text{Ct.Dia}}{2} \right)^3 \text{Ct.Th} \quad (2)$$

Following scanning, femora were wrapped in PBS-soaked gauze and stored at -20 °C until SAXS/WAXS testing.

2.4. Small and wide angle scattering

For X-ray analysis, a smaller subset of samples from each group were taken from the freezer an hour before preparation and thawed at room temperature, CON ($n = 3$), CON CAL ($n = 5$), CKD ($n = 7$), and CKD CAL ($n = 9$). To prepare for the scan, femoral heads were removed, and the bone marrow was flushed out with PBS. Samples were then placed in a sample holder with 20 cells each 4×4 mm² and sealed in Kapton tape (thickness $t = 0.14$ mm). Two background cells containing Kapton tape only were included in the sample array, at the start and the end of a sample run. The sample chamber was kept under a vacuum (3.0 mbar).

X-ray measurements were completed using a SAXSpoint 2.0 instrument (Anton Paar GmbH, Graz, Austria). The instrument was configured with a Primux 100 μ Cu K_{α} microfocus X-ray source ($\lambda = 0.154$ nm [8 keV]) with a beam diameter of 45 μ m with pin collimation. The read-out was from a 2D hybrid photon counting detector (area: 77.1×79.7 mm², pixel array: $1,028 \times 1,062$, pixel size: 75×75 μ m², flux magnitude: 10^8 ph/s, maximum count rate: 3.8×10^6 ph/s/pixel, point spread function full-width half maximum (FWHM): 1 pixel). The maximum radiation dose was kept below 35 kGy, to ensure collagen integrity, using an acquisition time of 15 s divided between 3 frames for each measurement spot (Barth et al., 2010). For each femur, three spots were measured with a distance of 0.2 mm between spot centers to account for the beam size, and data were averaged. The sample-to-detector distance for SAXS was 826 mm ($0.005 \leq q \leq 0.05$, \AA^{-1}) and for WAXS was 113 mm ($0.5 \leq q \leq 2.5$, \AA^{-1}). After measurements, samples were wrapped in gauze soaked in PBS and placed back in the freezer (-4 °C) until TgA characterization.

Data reduction was performed with a Python code (Bush et al., 2025). After reduction, 1D plots were analyzed in SasView (<https://>

[//www.sasview.org/](http://www.sasview.org/)). The thickness of the mineral platelets (T) was determined following the method in [Fratzl et al. \(1992\)](#) and uses Porod's scattering power law ($\sim q^{-4}$) and the total scattering volume Q . Invariant and correlation functions were used to find Q and Porod constant, C_p , respectively ([Butler and King, 2020](#); [King et al., 2020](#)):

$$T = \frac{4Q}{\pi C_p} \quad (3)$$

Meridional D -Periodicity was evaluated by applying a gaussian fit on the 3rd order bragg peak, where $q = 2\pi n/D$ and $n = 3$. A Lorentzian fit was applied to the mid-range values of q ($0.03 \leq q \leq 0.14, \text{\AA}^{-1}$) to model the spacing of collagen (ξ_{col}) ([Ornstein and Zernike, 1914](#)):

$$I(q) = \frac{A}{1 + (q\xi_{col})^2} + I_{Bg} \quad (4)$$

The applied scale factor (A) and background (I_{Bg}) are normalization factors for all Lorentzian fit models.

Mineral crystal dimensions were processed from WAXS measurements. To find the mineral lattice spacing (d) from the hydroxyapatite (002) peak (1.8\AA^{-1}), the peak was fit with a Gaussian function. The peak center was used in Bragg's law to find d . The standard deviation of the Gaussian function, σ , was used to find the FWHM (β) that satisfies the Scherrer equation. Then, the size of the mature crystal length along the c -axis, L , is obtained below:

$$L = \frac{K\lambda}{\beta \cos(\theta)} \quad (5)$$

Here, K is a shape factor ($0.6 < K < 1.0$), and is assigned as $K = 0.9$ as a common practice ([Turunen et al., 2016](#)).

2.5. Thermogravimetric analysis

The samples were thawed and blotted with KimWipe to remove excess PBS. The samples were subjected to thermographic analysis (TGA) (TGA 550, Waters TA Instruments, New Castle, DE, USA) at a temperature rate of $5 \text{ }^\circ\text{C}/\text{min}$ until a temperature of $T_e = 900 \text{ }^\circ\text{C}$ was reached. Data were processed numerically (OriginLab Corporation, Northampton, MA, USA) to obtain the first derivative of weight vs. temperature. The first derivative curve was used to evaluate and identify critical temperature values and temperature ranges for specific mass loss domains. The first peak in the derivative curve, T_1 , represents the temperature at which the loss rate of water is maximum. Mass loss at $T < T_1$ (35 to $60 \text{ }^\circ\text{C}$) is attributed to free water. All values are normalized to the wt.% of free water to ensure excess PBS is not falsely skewing the wt.% of other phases.

The second peak in the derivative curve, T_2 , ($\sim 330 \text{ }^\circ\text{C}$) represents the temperature at which the rate of organic matrix loss is a maximum. The midpoint temperature T_{12} is defined as $T_{12} = (T_1 + (T_2 - T_1))/2$. Mass loss associated with the temperature interval $[T_1, T_{12}]$ (~ 170 to $205 \text{ }^\circ\text{C}$) is associated with the loss of loosely bound water. The organic matrix mass was determined to be any loss between the end of the water phase (T_{12}) to the final mass at T_e . The final mass is attributed to the mineral mass as it is the only crystalline hydroxyapatite left at $900 \text{ }^\circ\text{C}$ ([Rodriguez-Florez et al., 2015](#); [Surowiec et al., 2022](#)). Gaussian fits were applied to the water and organic matrix peaks to identify peak maxima. To describe the matrix quality (ϕ), the following equation was used:

$$\phi = \frac{\text{Mineral wt.\%}}{\text{Collagen wt.\%} + \text{Bound Water wt.\%}} \quad (6)$$

2.6. Statistics

Statistical analysis was completed using the Python module statsmodels ([Seabold and Perktold, 2010](#)). Shapiro–Wilk normality tests were used to ensure that the groups could be used in a two-way ANOVA test for statistical significance between CON groups and CKD groups and to test the impact of treatment. For each outcome tested, p -values are reported and tested against an alpha of 0.05. For interaction effect significance, a Tukey HSD test was performed after the two-way ANOVA.

3. Results

3.1. Biochemistries

To confirm the presence of CKD, the serum levels of BUN and PTH were measured for each group. Shown in [Fig. 1\(a\)](#) and [Table 1](#) healthy bone had lower BUN levels than diseased bone (Disease: $p < 0.001$). The CON group had BUN levels of $34.42 \pm 10.30 \text{ mg/dL}$ compared to the CKD group with a level of $56.00 \pm 4.52 \text{ mg/dL}$. There was no significance that calcitonin affected serum BUN concentration, neither in the CON CAL group ($35.64 \pm 12.18 \text{ mg/dL}$) nor in the CKD CAL group ($56.72 \pm 12.25 \text{ mg/dL}$). Differences in serum PTH levels were reported in healthy versus diseased bone, in [Fig. 1\(b\)](#) (Disease: $p < 0.001$), with CON showing PTH levels of $426.92 \pm 174.01 \text{ pg/mL}$ and CKD of $1063 \pm 675.48 \text{ pg/mL}$. CAL did not affect serum PTH concentration as CON CAL had a value of $340.67 \pm 170.83 \text{ pg/mL}$ and CKD CAL a level of $907.65 \pm 442.51 \text{ pg/mL}$. Changes in serum BUN and PTH indicate the successful induction of CKD.

3.2. X-ray micro computed tomography data

Representative micro-CT images of femur sections of all four bone conditions are given in [Fig. 2](#). Data on Cortical μCT derived outcomes (T.Ar, Ct. Ar, Ct.Th) and bone geometric distribution (Ct.Po, BA/TA, CSMI) are given in [Fig. 3](#) and in [Table 2](#). The analysis found evidence that CKD reduces bone structure compared to healthy bone, i.e. expressed as T.Ar, Ct.Ar and Ct.Th. There was no evidence that CAL affected the respective parameters of bone structure.

Evaluation of cortical bone shows in [Fig. 3\(a\)](#) that T.Ar was significantly higher in healthy bone than disease bone (Disease: $p = 0.008$). As reported in [Table 2](#) CON had a T.Ar of $2.3 \pm 0.17 \text{ mm}^2$ and CKD had a T.Ar of $2.1 \pm 0.17 \text{ mm}^2$. The changes from treatment were not significant as seen in [Fig. 3\(a\)](#) and reported in [Table 2](#), as CON CAL had a T.Ar of $2.3 \pm 0.14 \text{ mm}^2$ and CKD CAL a T.Ar of $2.1 \pm 0.17 \text{ mm}^2$. Disease is also shown to have a main effect on Ct.Ar, shown in [Fig. 3\(b\)](#) (Disease: $p < 0.001$). As reported in [Table 2](#), CON had a Ct.Ar of $0.94 \pm 0.07 \text{ mm}^2$ and CKD a Ct.Ar of $0.73 \pm 0.06 \text{ mm}^2$. There was no evidence of a change to Ct.Ar with CAL, seen in [Fig. 3\(b\)](#), as CON CAL had a Ct.Ar of $0.89 \pm 0.07 \text{ mm}^2$ and CKD CAL had a Ct.Ar $0.73 \pm 0.06 \text{ mm}^2$. The disease was shown in [Fig. 3\(c\)](#) to affect Ct.Th (Disease: $p < 0.001$). Healthy CON had a Ct.Th of $0.17 \pm 0.01 \text{ mm}$ and CKD had a Ct.Th of $0.13 \pm 0.02 \text{ mm}$. Treatment did not show any changes to Ct.Th as CON CAL had a Ct.Th of $0.17 \pm 0.01 \text{ mm}$ and CKD CAL had a Ct.Th of $0.14 \pm 0.01 \text{ mm}$.

The analysis of cortical geometry found evidence that CKD negatively affects parameters compared to healthy bones, i.e. Ct.Po, BA/TA, CSMI. Shown in [Fig. 3\(d\)](#) CKD alters Ct.Po in comparison to CON (Disease: $p < 0.001$). As reported in [Table 2](#) CON had a Ct.Po of $0.27 \pm 0.11\%$ while CKD had a Ct. Po of $1.49 \pm 1.06\%$. This is an 18% increase in Ct.Po with disease. There was no evidence in the data that Ct.Po was affected by treatment, as CON CAL had a Ct.Po of $0.37 \pm 0.28\%$ and CKD CAL had a Ct.Po of $1.01 \pm 0.60\%$. As shown in [Fig. 3\(e\)](#), bone area fraction (BA/TA) was decreased in the CKD group versus CON (Disease: $p < 0.001$), as CON has a BA/TA of $40 \pm 2.2\%$ and CKD a BA/TA of $32 \pm 4.7\%$. The effects of treatment were insignificant as CON CAL had a BA/TA of $39 \pm 2.5\%$ and CKD CAL had a BA/TA of $35 \pm 2.4\%$. Data on bone section modulus CSMI in [Fig. 3\(f\)](#) reveal evidence of a reduction in CSMI in the CKD group in comparison to CON (Disease: $p < 0.001$), as CON had a CSMI of $0.35 \pm 0.05 \text{ mm}^4$ and CKD a CSMI of $0.26 \pm 0.06 \text{ mm}^4$. Calcitonin did not affect the CSMI in either group as CON CAL had a CSMI of $0.33 \pm 0.04 \text{ mm}^4$ and CKD CAL had a CSMI of $0.26 \pm 0.04 \text{ mm}^4$.

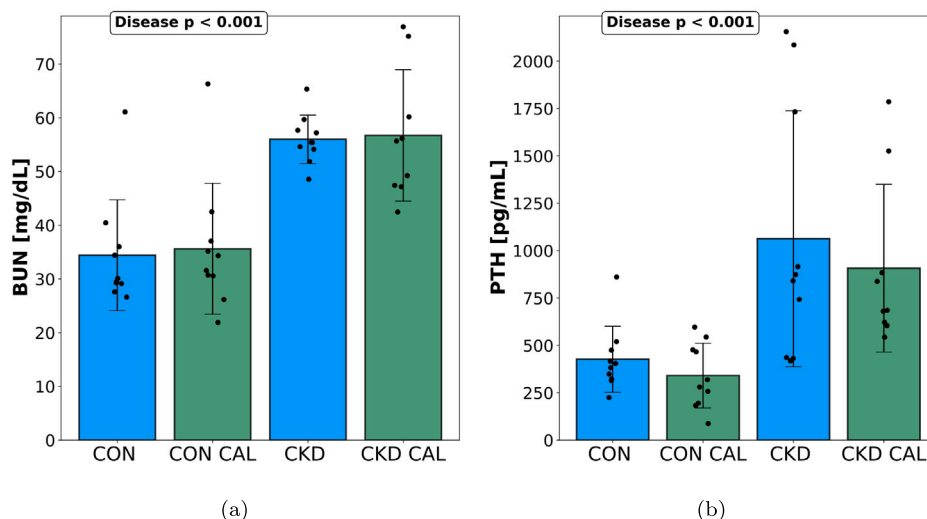


Fig. 1. Biochemical analysis: (a) Serum BUN concentration showing higher levels with CKD (Disease: $p < 0.001$) ; (b) Serum PTH concentration showing higher levels with CKD (Disease: $p < 0.001$).

Table 1

Means \pm standard deviations for serum biochemistry for BUN [mg/dL] and PTH [pg/mL] in the control and diseased samples. Results of two-way ANOVA tests and post-hoc analysis.

Serum	CON <i>n</i> = 10	CAL <i>n</i> = 10	CKD <i>n</i> = 10	CKD CAL <i>n</i> = 9	Group	Treatment	Interaction
BUN	34.42 \pm 10.30	35.64 \pm 12.18	56.00 \pm 4.52	56.72 \pm 12.25	$p < 0.001$	$p = 0.77$	$p = 0.94$
PTH	426.92 \pm 174.01	340.67 \pm 170.83	1063.27 \pm 675.48	907.65 \pm 442.51	$p < 0.001$	$p = 0.38$	$p = 0.80$

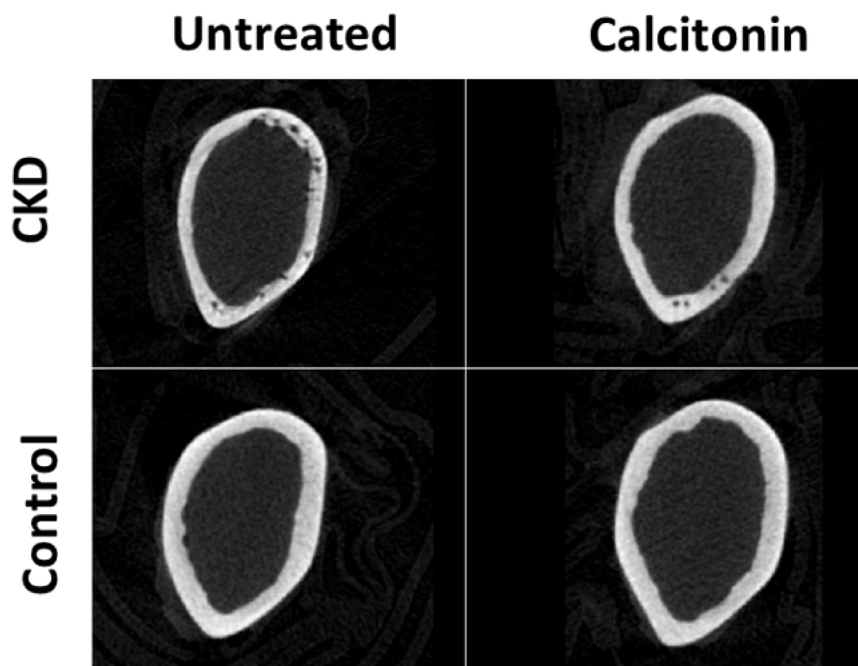


Fig. 2. Representative μ -CT based section images for each experimental group: CKD (top left), CKD CAL (top right), CON (bottom left), and CON CAL (bottom right). The deterioration in cortical bone due to chronic kidney disease is noticeable between the CKD and CON groups on the left side of the image. T.Ar, Ct. Po, Ct.Ar and Ct.Th are all significantly lower in CKD (top left) than CON (bottom left) as measured by μ -CT. There were no main effects measured from μ -CT seen in the images of calcitonin-treated groups CKD CAL (top right) and CON CAL (bottom right).

3.3. Small and wide angle scattering data

Representative 1D SAXS and WAXS curves are shown in Fig. 4. The q -ranges for the D-periodicity and Lorentz analysis are shown in the

top right and middle of the left columns, respectively. The plot in the bottom left represents the (002) peak of WAXS.

The mineral dimensions T , L and L/T , reported in Table 3 and shown in Fig. 5, are not affected by CKD or treatment. As shown in Fig. 5(a), the CON group had a T of 1.69 ± 0.18 nm and CKD had a T of

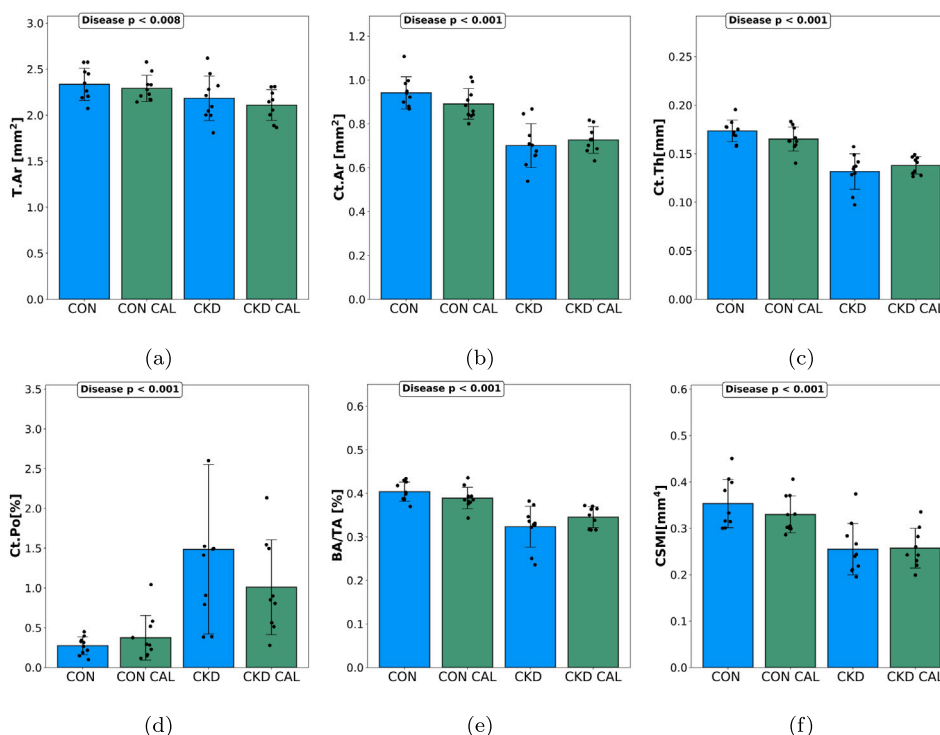


Fig. 3. Cortical μ CT derived outcomes: (a) T.Ar [mm²] was higher in CON and reduced with CKD (Disease: $p < 0.008$), (b) Ct.Ar [mm²] was higher in CON and reduced with CKD (Disease: $p < 0.001$), (c) Ct.Th [mm] was higher in CON and reduced with CKD (Disease: $p < 0.001$), (d) Ct.Po [%] was lower in CON and elevated with CKD (Disease: $p < 0.001$), (e) BA/TA [%] was higher in CON and reduced with CKD (Disease: $p < 0.001$), (f) CSMI [mm⁴] was higher in CON and reduced with CKD (Disease: $p < 0.001$).

Table 2

Means \pm standard deviations for μ CT derived quantities: T.Ar [mm²], Ct.Ar [mm²], Ct.Th [mm]. Bone geometry parameters: Ct.Po [%], BA/TA [%], CSMI [mm⁴]. Results of two-way ANOVA tests and post-hoc analysis.

Geometry	CON <i>n</i> = 10	CAL <i>n</i> = 10	CKD <i>n</i> = 10	CKD CAL <i>n</i> = 9	Group	Treatment	Interaction
T.Ar	2.3 \pm 0.17	2.3 \pm 0.14	2.2 \pm 0.24	2.1 \pm 0.17	$p = 0.008$	$p = 0.34$	$p = 0.80$
Ct.Ar	0.94 \pm 0.07	0.89 \pm 0.07	0.70 \pm 0.10	0.73 \pm 0.06	$p < 0.001$	$p = 0.59$	$p = 0.08$
Ct.Th	0.17 \pm 0.01	0.17 \pm 0.01	0.13 \pm 0.02	0.14 \pm 0.01	$p < 0.001$	$p = 0.77$	$p = 0.09$
Ct.Po	0.27 \pm 0.11	0.37 \pm 0.28	1.49 \pm 1.06	1.01 \pm 0.60	$p < 0.001$	$p = 0.38$	$p = 0.16$
BA/TA	40 \pm 2.2	39 \pm 2.5	32 \pm 4.7	35 \pm 2.4	$p < 0.001$	$p = 0.38$	$p = 0.08$
CSMI	0.35 \pm 0.05	0.33 \pm 0.04	0.26 \pm 0.06	0.26 \pm 0.04	$p < 0.001$	$p = 0.47$	$p = 0.41$

1.24 \pm 0.12 nm. For treated samples, CON CAL had a T of 1.49 \pm 0.16 nm while CKD CAL had a T of 1.48 \pm 0.34 nm. The length of the crystallite c axis, L , is shown in Fig. 5(b), CON was 34.3 \pm 3.82 nm long while CKD was 34.2 \pm 5.71 nm. For the treated groups, CON CAL had a length of 35.9 \pm 3.48 nm, and CKD CAL had a length of 36.5 \pm 1.57 nm. The mineral platelet aspect ratio, L/T , was calculated and reported in Fig. 5(c), although there was no disease effect, CON had a L/T of 22.8 \pm 2.8, and CKD had a L/T of 29.0 \pm 7.9. There was also no treatment effect for L/T , CON CAL had a ratio of 26.3 \pm 2.9, and CKD CAL had a ratio of 28.1 \pm 6.9.

The arrangement of the mineralized collagen matrix was analyzed by SAXS and WAXS. The D -Periodicity was not affected by disease. The D -Periodicity in CON was 65.9 \pm 3.73 nm, and for CKD 65.1 \pm 0.52 nm. Treatment had no effects on D -Periodicity, CON CAL 64.1 \pm 1.98 nm and CKD CAL 64.5 \pm 1.50 nm. Collagen helix spacings ξ_{col} are shown in Fig. 5(e) and reported in Table 3. Healthy CON had the largest spacing of 3.23 \pm 0.14 nm while CKD had the lowest at 2.54 \pm 0.22 nm (Disease: $p = 0.003$). Disease reduced the collagen spacing by approximately 22%. There was no evidence in the data that CAL affected this distance, as ξ_{col} of 3.27 \pm 0.80 nm for CON CAL and ξ_{col} of 2.70 \pm 0.20 nm for CKD CAL.

3.4. Thermogravimetric analysis data

Representative mass-temperature data from thermogravimetric experiments are shown in Fig. 6, with the respective first derivatives to accurately assess the material removal temperature intervals.

The matrix components evaluated from the TgA experiments are summarized in Fig. 7 and reported in Table 4. Mineral ratios are seen in Fig. 7(a), showing that mineral wt.%, in the CON groups, differed from that in the CKD groups, CON had a ratio of 65.9 \pm 3.0 wt.% and CKD a ratio of 67.8 \pm 1.0 wt.% (Disease: $p < 0.001$). However, CAL did not influence the mineral ratio as CON CAL had a ratio of 64.6 \pm 3.1 wt.% and CKD CAL had a ratio of 68.2 \pm 0.98 wt.%. The organic matrix ratios are shown in Fig. 7(b), and the main effects of CAL were reported. The organic matrix was unchanged by disease, CON had a wt.% of 21.6 \pm 0.90 wt.% while CKD had a wt.% of 21.8 \pm 0.72. There is evidence CAL increased the wt.% of the organic matrix for both CON vs. CON CAL and CKD vs. CKD CAL comparisons. The organic ratio for CON CAL was 22.7 \pm 1.06 wt.% and for CKD CAL 23.0 \pm 0.59 wt.% (Treatment: $p = 0.003$). The disease affected the hydration states of the bound water in the CKD group. Healthy bone in Fig. 7(c) had a higher amount of bound water with 12.5 \pm 3.53 wt.% while CKD had a wt.% of 10.3 \pm 1.42 wt.% (Disease: $p = 0.003$). There was no

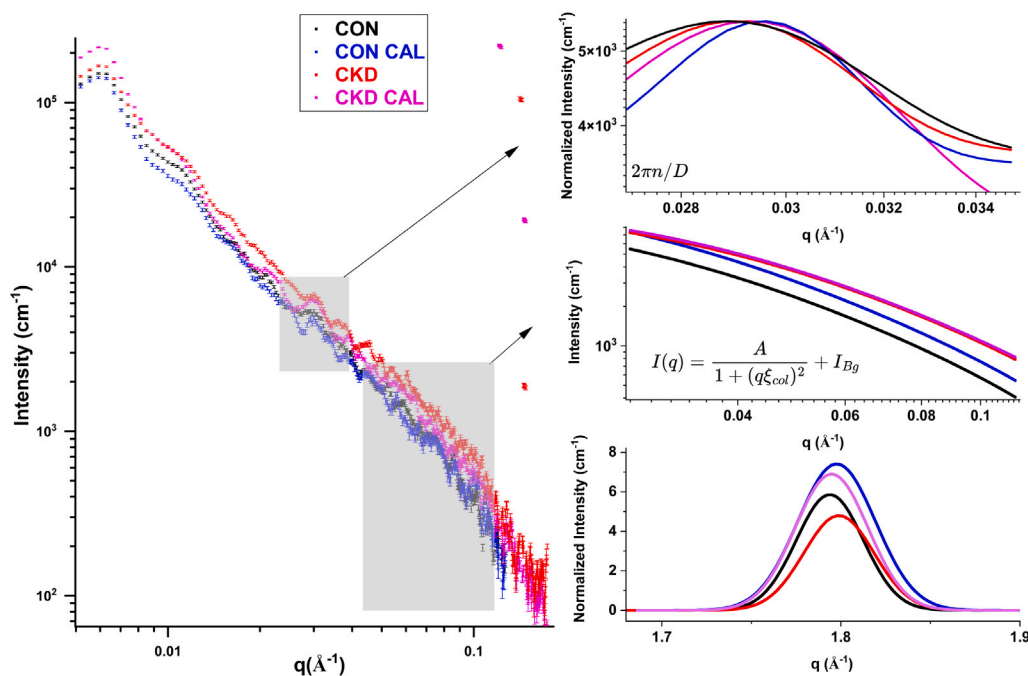


Fig. 4. 1D reduced SAXS $I - q$ data representative of CON, CKD, CON CAL, and CKD CAL groups (left). Meridional peak fits for D -periodicity are represented in the top right, while Lorentz fits for collagen spacing are represented in the middle left plot. 1D reduced WAXS $I - q$ data representative of CON, CKD, CON CAL, and CKD CAL groups normalized at the 1.8 \AA^{-1} peak representing mineral crystallite dimensions is shown in the bottom left.

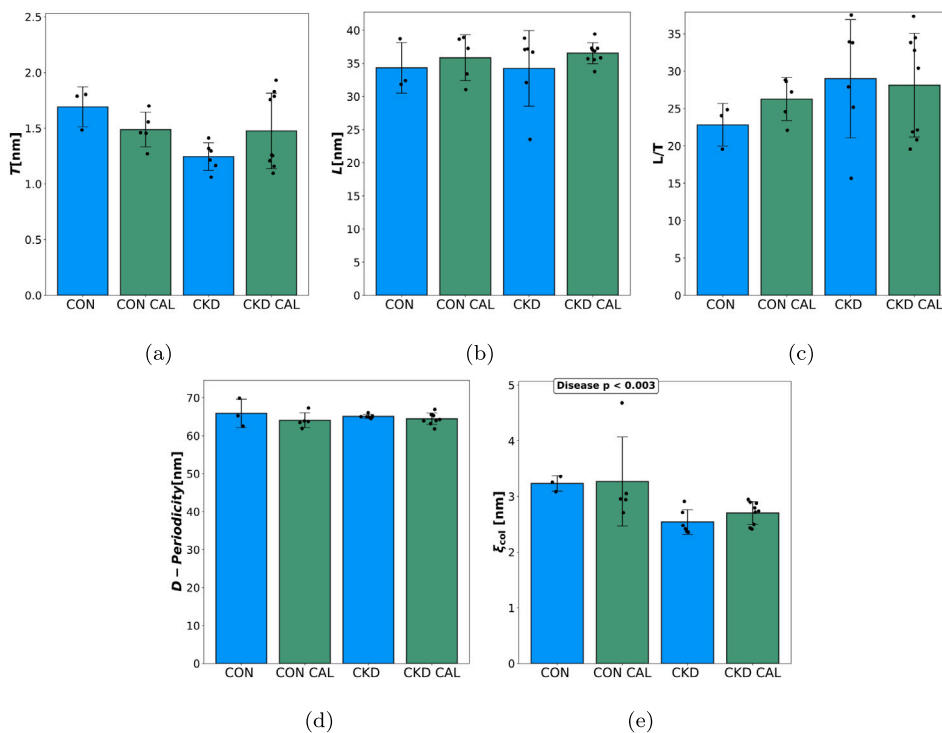


Fig. 5. SAXS and WAXS derived measured of the bone tissue nanostructure: (a) mineral platelet thickness T [nm] was unchanged by CKD or CAL, (b) mineral platelet length L [nm], (c) mineral platelet aspect ratio L/T was unchanged by CKD or CAL, (d) D -Periodicity was unchanged with disease or treatment, (e) collagen helix spacing ξ_{col} [nm] was higher in CON and reduced with CKD (Disease: $p = 0.003$).

evidence that calcitonin altered the loosely-bound water wt.% in either the CAL 12.7 ± 3.76 wt.% or CKD CAL 8.88 ± 0.69 wt.%. Matrix quality, ϕ , was analyzed in order to evaluate the shift in the matrix composition with disease and treatment. This ratio was shown to be affected by disease, as mineral content increased with disease shown in Fig. 7(d) and reported in Table 4.

4. Discussion

The results in this study are in line with previously reported outcomes of CKD on the cortical bone mass. We saw elevated levels of cortical porosity, lower cortical area, and thinner cortical walls from the impacts of CKD. There were also alterations to the cortical

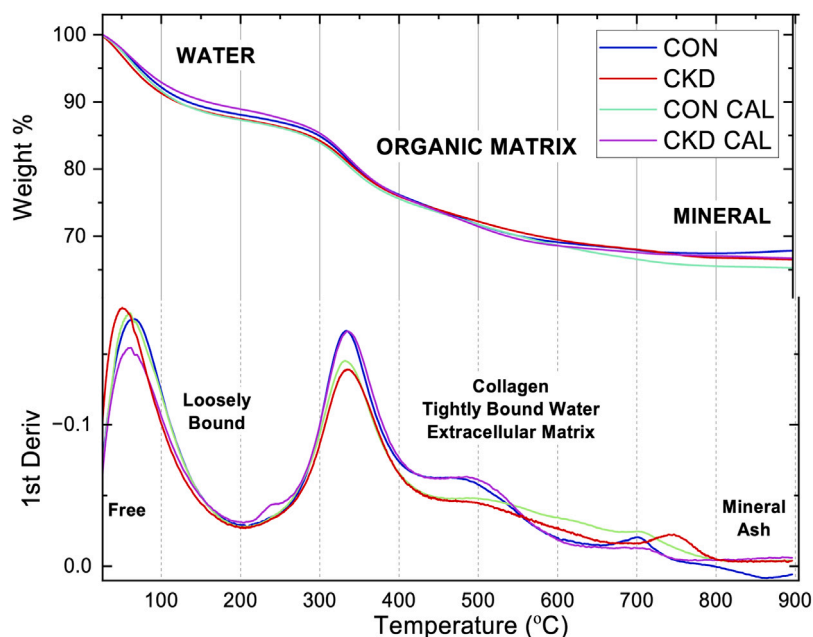


Fig. 6. Representative weight-temperature curves and respective first derivatives for CON, CKD, CON CAL, and CKD CAL. The first peak in the derivative curve represents the temperature at which the rate of loss of water is maximum, T_1 . Mass loss at $T < T_1$ (35 to 60 °C) is attributed to free water. The second peak in the derivative curve, T_2 , (~330 °C) represents the temperature at which the rate of organic matrix loss is a maximum. The midpoint temperature T_{12} is associated with the loss of loosely bound water. The final mass is attributed to the mineral mass as it is the only crystalline hydroxyapatite left at 900 °C.

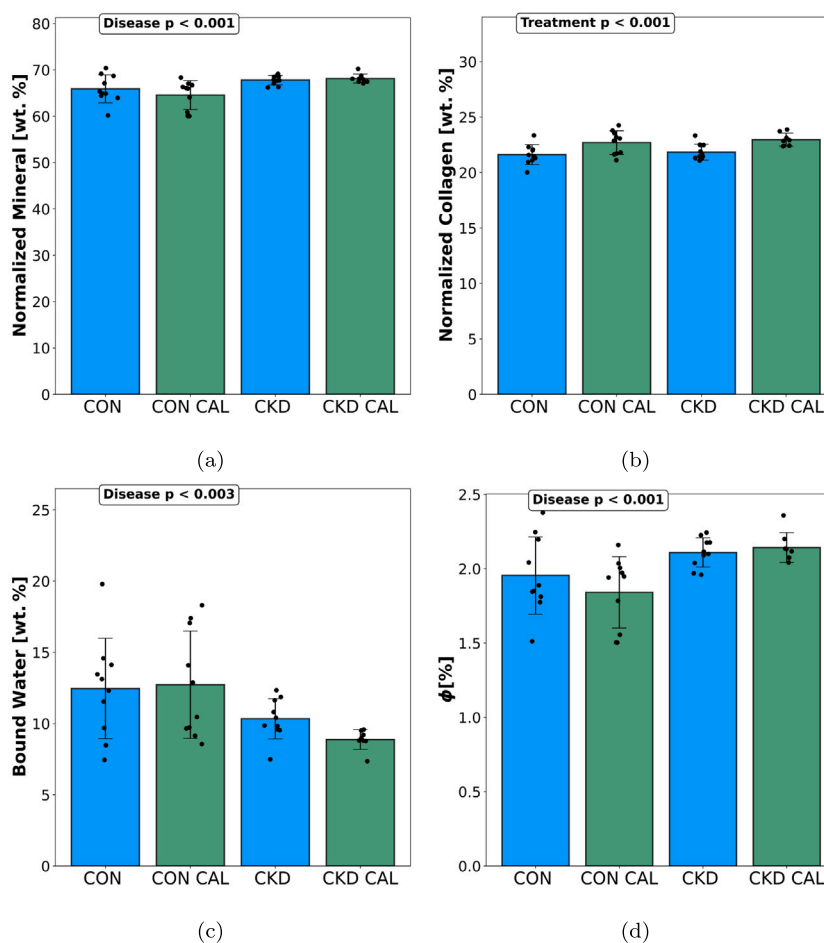


Fig. 7. TgA data: (a) mineral wt.% was lower in CON than in CKD groups (Disease: $p < 0.001$); (b) organic wt.% was unchanged by disease and increased with CAL (Treatment: $p = 0.003$) (c) Free and Loosely bound water wt.% was higher in CON than in CKD groups (Disease: $p = 0.003$); (d) matrix quality, ϕ , was impacted by both disease and treatment (Disease: $p < 0.001$).

Table 3

Means \pm standard deviations for SAXS and WAXS model fit parameters: mineral platelet thickness T [nm], mineral platelet length L [nm], mineral platelet aspect ratio L/T ; nanostructural D -Periodicity [nm], and collagen spacing ξ_{col} [nm]. Results of the two-way ANOVA test and post-hoc analysis.

Nanoscale Feature	CON $n = 3$	CAL $n = 5$	CKD $n = 6$	CKD CAL $n = 9$	Group	Treatment	Interaction
T	1.69 \pm 0.18	1.49 \pm 0.16	1.24 \pm 0.12	1.48 \pm 0.34	$p = 0.11$	$p = 0.45$	$p = 0.07$
L	34.3 \pm 3.82	35.9 \pm 3.48	34.2 \pm 5.71	36.5 \pm 1.57	$p = 0.43$	$p = 0.31$	$p = 0.82$
L/T	22.8 \pm 2.8	26.3 \pm 2.9	29.0 \pm 7.9	28.1 \pm 6.9	$p = 0.21$	$p = 0.82$	$p = 0.46$
D - periodicity	65.9 \pm 3.73	64.1 \pm 1.98	65.1 \pm 0.52	64.5 \pm 1.50	$p = 0.94$	$p = 0.21$	$p = 0.47$
ξ_{col}	3.23 \pm 0.14	3.27 \pm 0.80	2.54 \pm 0.22	2.70 \pm 0.20	$p = 0.003$	$p = 0.44$	$p = 0.75$

Table 4

Means \pm standard deviations for TgA results: Mineral [wt.%], Collagen [wt.%], Water [wt.%], and matrix quality, ϕ [%]. Results of the two-way ANOVA test and post-hoc analysis.

Phase	CON $n = 10$	CAL $n = 10$	CKD $n = 10$	CKD CAL $n = 9$	Group	Treatment	Interaction
Mineral	65.9 \pm 3.0	64.6 \pm 3.1	67.8 \pm 0.98	68.2 \pm 1.0	$p = 0.001$	$p = 0.47$	$p = 0.27$
Collagen	21.6 \pm 0.90	22.7 \pm 1.06	21.8 \pm 0.72	23.0 \pm 0.59	$p = 0.38$	$p = 0.003$	$p = 0.95$
Bound Water	12.5 \pm 3.53	12.7 \pm 3.76	10.34 \pm 1.42	8.88 \pm 0.69	$p = 0.003$	$p = 0.55$	$p = 0.34$
ϕ	1.95 \pm 0.26	1.84 \pm 0.24	2.14 \pm 0.10	2.11 \pm 0.10	$p = 0.001$	$p = 0.48$	$p = 0.25$

geometry, as a lower moment of inertia was reported. Elevated cortical porosity (Lau et al., 2013; McNerny et al., 2019; Metzger et al., 2022; Newman et al., 2023; Tippen et al., 2022) and decreased cortical thickness (Lee et al., 2010; Heveran et al., 2016a, 2019; Moe et al., 2014; Newman et al., 2014) and reduced cortical area (Newman et al., 2014; Metzger et al., 2020; Tippen et al., 2022; Swallow et al., 2022; Newman et al., 2023; Moe et al., 2014) have all been reported as outcomes from CKD. These changes in cortical micro-architecture are associated with reduced overall mechanical properties (Surowiec et al., 2023; Heveran et al., 2019; Newman et al., 2014). Lowered toughness and modulus were reported for CKD bone (Surowiec et al., 2023), toughness fell from ~ 8 MPa in CON bone to a toughness of ~ 3 to 4 MPa in CKD bone. Modulus also decreased with CKD, from ~ 2.5 GPa to ~ 1.5 GPa. Treatment with CAL had no statistical impact on improving the microstructure of bone. Although porosity was decreased in treated CKD bone, the variances were too large and CAL had the opposite effect in healthy bone to show a statistical change.

This study shows that the mineral wt.% in CKD increases compared to CON, as CON has a higher wt.% loosely bound water compared to CKD. The shift in hydration accentuates the mineral ratio in CKD bone. Prior studies of CKD (Allen et al., 2015; Iwasaki et al., 2011, 2015; Heveran et al., 2016b, 2019) have also documented changes to hydration and mineral content. This study showed that in-vivo treatment with CAL increased the wt.% of the organic matrix. We reported CAL did not alter mineral wt.% or free and loosely bound water Table 4. Then, an increase in the organic matrix wt.% is likely associated with the increase in tightly bound water relative to total hydration in the bone, representing a net redistribution of water from loosely to tightly bound water. Ex vivo exposure to CAL (Surowiec et al., 2023) was shown to increase the cortical-bound water from CKD conditions, which is believed to play a role in increasing the toughness of CKD bone. Ex vivo exposure to CAL improved toughness in CKD bone to ~ 8 MPa.

Here, we find a smaller linear distance between collagen domains in the CKD group than in the CON group, which could be a sign of collapsed collagen in CKD bone. We interpret the dimensional changes in nanoscale collagen domains to manifest as embrittlement, supporting the reported loss in toughness in CKD bone. The lack of hydration in the CKD bone compared to the healthy bone leads to a decrease in the water-to-mineral ratio. Compact collagen can reduce the interface for bound water. The reduced collagen-to-collagen spacing, ξ_{col} , suggests a decrease in the total volume in the organic matrix at the nanoscale compared to that in the CON group. The lack of alteration in the thickness or length of individual mineral platelets shows that there are no changes in the mineral quality, but mainly in the mineral-organic

arrangement at the nanoscale. We see no significant changes in the D -Periodicity of CKD bone compared to that of the control. In a previous study (Heveran et al., 2019), in-situ tensile testing was performed using SAXS to analyze the changes in bone quality with CKD. It was shown that collagen % strain at the maximum applied strain on the tissue was greater in CKD bones than in healthy bones. Although the direct reason for the alteration of the collagen mechanics with CKD is unknown, reduced whole bone toughness, changes in collagen cross-linking, and mineral rearrangement were suggested.

Fig. 8 provides a schematic visualization of the bone characteristics from SAXS/WAXS data and the interpretation of the TgA measurements.

Study limitations in the mouse model include the use of only male mice, cortical bone and not trabecular and, the consideration of only one dosage and treatment regime. These shortcomings restrain the ability to draw any conclusions regarding, gender and site specific effects by disease or treatment on the overall bone quantity. Insufficient biochemical data also limits the ability for any finite conclusion on calcitonin's physiological mechanisms to alter or change bone turnover, based on analysis of serum biomarkers. The biochemical data provided is limited to showing that CKD had been induced. The lack of biomechanical data is another limitation, as we are only able to use findings from previous studies to narrowly understand how the outcomes from calcitonin could improve the fracture toughness in bone. Other limitations arise from the SAXS and WAXS measurements. Data collection is conducted under vacuum, with Kapton tape used to seal hydration in the sample. Multiple data fitting models were needed to interpret the structural changes between sample groups due to the similarity of mineral and collagen phases potentially leading to variances in the data that are greater than other techniques presented here. The difference in sample size for SAXS from the other techniques also impacted the ability to see changes between the control and CKD groups with statistical analysis.

5. Conclusion

This study sought to investigate the mechanisms by which calcitonin treatment affects long bones. Using the in vivo mouse model of chronic kidney disease, the effects of calcitonin at a specified dose on both healthy and diseased bone were investigated. The study leads to the following findings:

- Chronic Kidney Disease affects bone quantity (cortical area, cortical thickness), cortical bone microstructure (cortical porosity), and cortical geometry (cross-section moment of inertia).
- Chronic kidney disease altered the collagen-mineral arrangement by reducing the nanoscale spacing between collagen fibers.

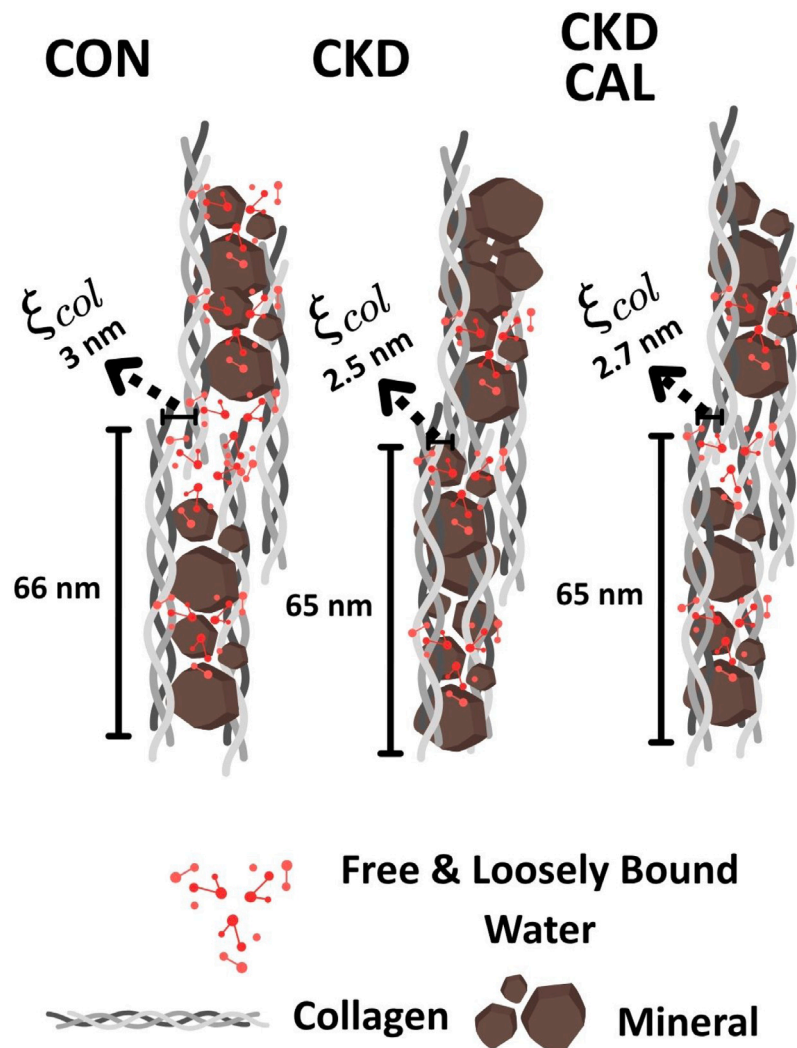


Fig. 8. Bone nanostructure: mineral platelets, collagen, and free and loosely bound water are represented above in group CON, CKD, and CKD CAL groups to demonstrate the impact of disease and treatment on diseased bone. The corresponding lengths measured by SAXS are labeled. The matrix quality is shown in CKD to have a higher mineral ratio compared to the healthy bone (CON) and disease-treated bone (CKD CAL) by showing more mineral platelets in the diseased (CKD) schematic.

- Chronic kidney disease shifts the quantity of each phase in the mineralized matrix. There is a reduction of free and loosely bound water, which increases the ratio of mineral and collagen.
- Calcitonin increases the ratio of the organic matrix in healthy and diseased bone.
- Calcitonin does not affect bone quantity, cortical microstructure, and cortical geometry.

CRediT authorship contribution statement

E. Montagnino: Writing – review & editing, Writing – original draft, Methodology, Investigation, Formal analysis, Data curation. **W. Bush:** Software, Methodology, Investigation, Data curation. **J. Bustamante:** Resources, Methodology, Conceptualization. **W. Bandara:** Methodology, Investigation, Data curation. **P. Jalaie:** Methodology, Investigation, Formal analysis, Data curation. **M.R. Allen:** Writing – review & editing, Resources, Methodology, Conceptualization. **J.M. Wallace:** Writing – review & editing, Writing – original draft, Supervision, Resources, Project administration, Methodology, Investigation, Funding acquisition, Conceptualization. **T. Siegmund:** Writing – review & editing, Writing – original draft, Supervision, Resources, Project administration, Investigation, Funding acquisition, Formal analysis. **R.K.**

Surowiec: Writing – review & editing, Writing – original draft, Supervision, Resources, Project administration, Methodology, Investigation, Funding acquisition, Formal analysis, Data curation, Conceptualization. **J.A. Howarter:** Writing – review & editing, Writing – original draft, Supervision, Resources, Methodology, Formal analysis, Data curation.

Declaration of competing interest

The authors declare that they have no known competing financial interests or personal relationships that could have appeared to influence the work reported in this paper.

Acknowledgments

This work was supported by the National Science Foundation [LEAP-HI 1952993 (TS, JAH, JMW, MRA)] and the National Institutes of Health [LRP 1L30DK130133-0 (RKS) and NIAMS R01AR072609 (JMW)]. This work benefited from the use of the SasView application, originally developed under NSF award DMR-0520547. SasView contains code developed with funding from the European Union's Horizon 2020 research and innovation programme under the SINE2020 project, grant agreement No. 654000.

Data availability

Data for this manuscript can be found at Purdue University Research Repository.

Supporting data for "Nanostructural Changes in Bone Quality in a Mouse Model of Chronic Kidney Disease and Treatment with Calcitonin (Original data) (The Purdue University Research Repository (PURR)).

References

- Allen, M.R., Newman, C.L., Chen, N., Granke, M., Nyman, J.S., Moe, S.M., 2015. Changes in skeletal collagen cross-links and matrix hydration in high- and low-turnover chronic kidney disease. *Osteoporosis International* 26 (3), 977–985. <http://dx.doi.org/10.1007/S00198-014-2978-9>.
- Barth, H.D., Launey, M.E., MacDowell, A.A., Ager, J.W., Ritchie, R.O., 2010. On the effect of X-ray irradiation on the deformation and fracture behavior of human cortical bone. *Bone* 46 (6), 1475–1485. <http://dx.doi.org/10.1016/j.bone.2010.02.025>.
- Battaglia, T.C., Tsou, A.C., Taylor, E.A., Mikic, B., 2003. Ash Content Modulation of Torsionally Derived Elastic Material Properties in Cortical Mouse Bone. *J. Biomech. Eng.* 125 (5), 615–619. <http://dx.doi.org/10.1115/1.1611513>.
- Bush, W.D., Montagnino, E.S., Siegmund, T.H., Howarter, J.A., 2025. Code for Processing Laboratory SAXS/WAXS Data in NEXUS File Format. Purdue University Research Repository. <http://dx.doi.org/10.4231/A21M-D344>.
- Butler, P., King, S., 2020. Invariant Calculation — SasView 5.0.6 documentation.
- Chesnut, C.H., Silverman, S., Andriano, K., Genant, H., Gimona, A., Harris, S., Kiel, D., Leboff, M., Maricic, M., Miller, P., Moniz, C., Peacock, M., Richardson, P., Watts, N., Baylink, D., 2000. A randomized trial of nasal spray salmon calcitonin in postmenopausal women with established osteoporosis: The prevent recurrence of osteoporotic fractures study. *American Journal of Medicine* 109 (4), 267–276. [http://dx.doi.org/10.1016/S0002-9343\(00\)00490-3](http://dx.doi.org/10.1016/S0002-9343(00)00490-3).
- Chiu, H.W., Hou, Y.C., Lu, C.L., Lu, K.C., Liu, W.C., Shyu, J.F., Chang, J.F., Zheng, C.M., 2022. Cincalcet Improves Bone Parameters Through Regulation of Osteoclast Endoplasmic Reticulum Stress, Autophagy, and Apoptotic Pathways in Chronic Kidney Disease—Mineral and Bone Disorder. *J. Bone Miner. Res.* 37 (2), 215–225. <http://dx.doi.org/10.1002/JBMR.4459>.
- Currey, J.D., 1969. The mechanical consequences of variation in the mineral content of bone. *J. Biomech.* 2 (1), 1–11. [http://dx.doi.org/10.1016/0021-9290\(69\)90036-0](http://dx.doi.org/10.1016/0021-9290(69)90036-0).
- Fratzl, P., Groschner, M., Vogl, G., Plenk, H., Eschberger, J., Fratzl-Zelman, N., Koller, K., Klaushofer, K., 1992. Mineral crystals in calcified tissues: A comparative study by SAXS. *J. Bone Miner. Res.* 7 (3), 329–334. <http://dx.doi.org/10.1002/JBMR.5650070313>.
- Henriksen, K., Byrjalsen, I., Andersen, J.R., Bihlet, A.R., Russo, L.A., Alexandersen, P., Valter, I., Qvist, P., Lau, E., Riis, B.J., Christiansen, C., Karsdal, M.A., 2016. A randomized, double-blind, multicenter, placebo-controlled study to evaluate the efficacy and safety of oral salmon calcitonin in the treatment of osteoporosis in postmenopausal women taking calcium and vitamin D. *Bone* 91, 122–129. <http://dx.doi.org/10.1016/j.bone.2016.07.019>.
- Heveran, C.M., Livingston, E., Bateman, T., Levi, M., King, K.B., Ferguson, V.L., 2016a. The effect of CKD on bone quality is greater for old than young C57Bl/6 mice. *J. Orthop. Res.* 34 (Supplement 1).
- Heveran, C.M., Ortega, A.M., Cureton, A., Clark, R., Livingston, E.W., Bateman, T.A., Levi, M., King, K.B., Ferguson, V.L., 2016b. Moderate chronic kidney disease impairs bone quality in C57Bl/6J mice. *Bone* 86, 1–9. <http://dx.doi.org/10.1016/j.bone.2016.02.006>.
- Heveran, C.M., Schurman, C.A., Acevedo, C., Livingston, E.W., Howe, D., Schaible, E.G., Hunt, H.B., Rauff, A., Donnelly, E., Carpenter, R.D., Levi, M., Lau, A.G., Bateman, T.A., Alliston, T., King, K.B., Ferguson, V.L., 2019. Chronic kidney disease and aging differentially diminish bone material and microarchitecture in C57Bl/6 mice. *Bone* 127, 91–103. <http://dx.doi.org/10.1016/J.BONE.2019.04.019>.
- Iwasaki, Y., Kazama, J.J., Yamato, H., Fukagawa, M., 2011. Changes in chemical composition of cortical bone associated with bone fragility in rat model with chronic kidney disease. *Bone* 48 (6), 1260–1267. <http://dx.doi.org/10.1016/j.bone.2011.03.672>.
- Iwasaki, Y., Kazama, J.J., Yamato, H., Matsugaki, A., Nakano, T., Fukagawa, M., 2015. Altered material properties are responsible for bone fragility in rats with chronic kidney injury. *Bone* 81, 247–254. <http://dx.doi.org/10.1016/j.bone.2015.07.015>.
- King, S., Rozyczko, P., Potrzebowski, W., 2020. Correlation Function Analysis—SasView 5.0.6 documentation.
- Lau, W.L., Linnes, M., Chu, E.Y., Foster, B.L., Bartley, B.A., Somerman, M.J., Giachelli, C.M., 2013. High phosphate feeding promotes mineral and bone abnormalities in mice with chronic kidney disease. *Nephrol. Dial. Transplant* 28 (1), 62–69. <http://dx.doi.org/10.1093/NDT/GFS333>.
- Lee, M.M., Chu, E.Y., El-Abbadi, M.M., Foster, B.L., Tompkins, K.A., Giachelli, C.M., Somerman, M.J., 2010. Characterization of Mandibular Bone in a Mouse Model of Chronic Kidney Disease. *J. Clin. Periodontol.* 81 (2), 300–309. <http://dx.doi.org/10.1902/JOP.2009.090379>, <https://aap.onlinelibrary.wiley.com/doi/10.1902/jop.2009.090379>.
- Lopez Franco, G.E., Blank, R.D., Akhter, M.P., 2011. Intrinsic material properties of cortical bone. *J. Bone Miner. Metabol.* 29 (1), 31–36. <http://dx.doi.org/10.1007/S00774-010-0194-Z/FIGURES/4>, <https://link.springer.com/article/10.1007/s00774-010-0194-z>.
- McNerny, E.M., Buening, D.T., Aref, M.W., Chen, N.X., Moe, S.M., Allen, M.R., 2019. Time course of rapid bone loss and cortical porosity formation observed by longitudinal μ CT in a rat model of CKD. *Bone* 125, 16. <http://dx.doi.org/10.1016/J.BONE.2019.05.002>, <https://pubmed.ncbi.nlm.nih.gov/articles/PMC6581598/>.
- Metzger, C.E., Newman, C.L., Tippen, S.P., Golemme, N.T., Chen, N.X., Moe, S.M., Allen, M.R., 2022. Cortical porosity occurs at varying degrees throughout the skeleton in rats with chronic kidney disease. *Bone Rep.* 17, 101612. <http://dx.doi.org/10.1016/j.bonr.2022.101612>.
- Metzger, C.E., Swallow, E.A., Allen, M.R., 2020. Elevations in Cortical Porosity Occur Prior to Significant Rise in Serum Parathyroid Hormone in Young Female Mice with Adenine-Induced CKD. *Calcif. Tissue Int.* 106 (4), 392–400. <http://dx.doi.org/10.1007/s00223-019-00642-w>.
- Moe, S.M., Chen, N.X., Newman, C.L., Gattone, V.H., Organ, J.M., Chen, X., Allen, M.R., 2014. A comparison of calcium to zoledronic acid for improvement of cortical bone in an animal model of CKD. *J. Bone Miner. Res.* 29 (4), 902–910. <http://dx.doi.org/10.1002/JBMR.2089>.
- Newman, C.L., Moe, S.M., Chen, N.X., Hammond, M.A., Wallace, J.M., Nyman, J.S., Allen, M.R., 2014. Cortical bone mechanical properties are altered in an animal model of progressive chronic kidney disease. *PLoS One* 9 (6), e99262. <http://dx.doi.org/10.1371/JOURNAL.PONE.0099262>.
- Newman, C.L., Surowiec, R.K., Swallow, E.A., Metzger, C.E., Kim, J., Tomaschke, A.A., Chen, N.X., Allen, M.R., Wallace, J.M., Moe, S.M., Wu, Y.C., Niziolek, P.J., 2023. Assessing cortical bone porosity with MRI in an animal model of chronic kidney disease. *Bone* 173, 116808. <http://dx.doi.org/10.1016/J.BONE.2023.116808>.
- Nickolas, T.L., Leonard, M.B., Shane, E., 2008. Chronic kidney disease and bone fracture: A growing concern. *Kidney Int.* 74 (6), 721–731. <http://dx.doi.org/10.1038/KI.2008.264>.
- Nickolas, T.L., Stein, E.M., Dworakowski, E., Nishiyama, K.K., Komandah-Kossef, M., Zhang, C.A., McMahon, D.J., Liu, X.S., Boutroy, S., Cremers, S., Shane, E., 2013. Rapid cortical bone loss in patients with chronic kidney disease. *J. Bone Miner. Res.* 28 (8), 1811–1820. <http://dx.doi.org/10.1002/JBMR.1916>.
- Ornstein, S., Zernike, F., 1914. Accidental deviations of density and opalescence at the critical point of a single substance. *Proc. Nat. Acad. Sci. Ams.* 17, 793–806.
- Rodriguez-Florez, N., Garcia-Tunon, E., Mukadam, Q., Saiz, E., Oldknow, K.J., Farquharson, C., Millán, J.L., Boyde, A., Shefelbine, S.J., 2015. An Investigation of the Mineral in Ductile and Brittle Cortical Mouse Bone. *J. Bone Miner. Res.* 30 (5), 786–795. <http://dx.doi.org/10.1002/JBMR.2414>.
- Seabold, S., Perktold, J., 2010. statsmodels: Econometric and statistical modeling with python. In: *9th Python in Science Conference*.
- Sharma, S., Kumar, S., Tomar, M.S., Chauhan, D., Kulkarni, C., Rajput, S., Sadhukhan, S., Porwal, K., Guha, R., Shrivastava, A., Gayen, J.R., Kumar, N., Chattopadhyay, N., 2024. Multiscale effects of the calcimimetic drug, etelcalcetide on bone health of rats with secondary hyperparathyroidism induced by chronic kidney disease. *Bone* 185, 117126. <http://dx.doi.org/10.1016/J.BONE.2024.117126>, <https://www.sciencedirect.com/science/article/abs/pii/S8756328224001157>.
- Surowiec, R.K., Allen, M.R., Wallace, J.M., 2022. Bone hydration: How we can evaluate it, what can it tell us, and is it an effective therapeutic target? *Bone Rep.* 16, 101161. <http://dx.doi.org/10.1016/j.bonr.2021.101161>.
- Surowiec, R.K., Reul, O.N., Chowdhury, N.N., Rai, R.K., Segvich, D., Tomaschke, A.A., Dmrath, J., Jacobson, A.M., Allen, M.R., Wallace, J.M., 2024. Combining raloxifene and mechanical loading improves bone composition and mechanical properties in a murine model of chronic kidney disease (CKD). *Bone* 183, 117089. <http://dx.doi.org/10.1016/j.bone.2024.117089>.
- Surowiec, R.K., Saldivar, R., Rai, R.K., Metzger, C.E., Jacobson, A.M., Allen, M.R., Wallace, J.M., 2023. Ex vivo exposure to calcitonin or raloxifene improves mechanical properties of diseased bone through non-cell mediated mechanisms. *Bone* 173, 116805. <http://dx.doi.org/10.1016/j.bone.2023.116805>.
- Swallow, E.A., Metzger, C.E., Newman, C.L., Chen, N.X., Moe, S.M., Allen, M.R., 2022. Cortical porosity development and progression is mitigated after etelcalcetide treatment in an animal model of chronic kidney disease. *Bone* 157, <http://dx.doi.org/10.1016/J.BONE.2022.116340>.
- Tippen, S.P., Metzger, C.E., Swallow, E.A., Sacks, S.A., Wallace, J.M., Allen, M.R., 2022. The combination of aging and chronic kidney disease leads to an exacerbated cortical porosity phenotype. *Bone* 154, <http://dx.doi.org/10.1016/j.bone.2021.116228>.
- Turunen, M.J., Kaspersen, J.D., Olsson, U., Guizar-Sicarios, M., Bech, M., Schaff, F., Tägil, M., Jurvelin, J.S., Isaksson, H., 2016. Bone mineral crystal size and organization vary across mature rat bone cortex. *J. Struct. Biol.* 195 (3), 337–344. <http://dx.doi.org/10.1016/J.JSB.2016.07.005>.
- Wagermaier, W., Klaushofer, K., Fratzl, P., 2015. Fragility of Bone Material Controlled by Internal Interfaces. *Calcif. Tissue Int.* 97 (3), 201–212. <http://dx.doi.org/10.1007/s00223-015-9978-4>.
- Weiner, S., Wagner, H.D., 1998. The material bone: structure mechanical function relations. *Annu. Rev. Mater. Sci.* 28 (1), 271–298. <http://dx.doi.org/10.1146/annurev.matsci.28.1.271>.
- Zalozyc, A., Bernardor, J., Bacchetta, J., Laverny, G., Schmitt, C.P., 2023. Mouse Models of Mineral Bone Disorders Associated with Chronic Kidney Disease. *Int. J. Mol. Sci.* 24 (6), 5325. <http://dx.doi.org/10.3390/IJMS24065325>, <https://pubmed.ncbi.nlm.nih.gov/articles/PMC10048881/>.